JMEPEG (2019) 28:5843–5849
https://doi.org/10.1007/s11665-019-04302-w

1059-9495/$19.00

Microstructure Evolution and Improved Creep Behavior of Mg-Al-Si Alloy Matrix Composite Reinforced with SiC Nanoparticles

Ming Li, Gaozhan Zhao, Zhiwei Huang, Jianquan Tao, Yuanyuan Wan, Zhihui Xing, Hongxia Wang, and Qiang Chen

(Submitted November 8, 2018; in revised form April 15, 2019; published online September 6, 2019)

The Mg-9Al-1Si matrix composite reinforced with SiC nanoparticles is fabricated by semisolid stirring-assisted ultrasonic vibration, which contains finer grains and a more uniform microstructure compared to that of the Mg-9Al-1Si alloys. The sizes of the $Mg_{17}Al_{12}$ and Mg_2Si phases decreased continuously as the volume fraction of n-SiCp increased from 0 to 1% and then increased apparently when the volume fraction of n-SiCp increased to 1.5%. The steady-creep rates of the 1 vol.% n-SiCp/Mg-9Al-1Si are approximately two times lower than those of the Mg-9Al-1Si matrix alloy at 200 °C under applied stress of 70 MPa due to the strengthening effect of the nanosized SiCp. The reason for the improved creep properties is mainly attributed to the obvious grain boundary strengthening, the Orowan strengthening mechanism, the load transfer effect, and the pinning effect of the n-SiCp and the refined $Mg_{17}Al_{12}$ and Mg_2Si phases.

Keywords creep resistance, magnesium matrix composite, microstructure, SiC nanoparticles, strengthening mechanism

1. Introduction

Magnesium (Mg) alloys are promising light-weight structural materials for application in defense, automobile and aerospace industries, where a weight reduction is critical (Ref 1–5). Mg-Al-based alloys is the most commonly used Mg alloys, particularly the AZ91Mg alloy, due to their superior castability and wide range of mechanical properties at room temperature (Ref 6, 7). However, the application of these alloys is still limited to low temperatures due to the low thermal stability of the microstructure, which contains the net-shaped $Mg_{17}Al_{12}$ precipitates along grain boundaries. In the AZ91 alloy, in addition to the coarsening and dissolution of $Mg_{17}Al_{12}$ precipitates at high temperatures, cellular discontinuous precipitation of this phase can also deteriorate the creep resistance during aging. Studies have reported that this type of precipitation multiplies the grain boundary area, providing more surfaces for easy deformation regimes such as grain boundary sliding at high temperatures (Ref 8, 9). Therefore, improving the elevated temperature mechanical properties has become a critical issue to enable the application of Mg-Al-based alloys at higher temperatures. Most of these efforts have focused on restraining the discontinuous precipitation of $Mg_{17}Al_{12}$ and forming thermally stable phases in the Mg matrix for improving the creep behavior of the AZ91 alloy. Asl et al. (Ref 10) studied the effects of Si additions on the creep properties of AZ91 at 200 °C and found that AZ91 with 1 wt.% Si showed great improvement in the creep properties compared to those of the original AZ91 alloy, essentially because of the presence of a thermally stable Mg_2Si intermetallic phase. Srinivasan et al. (Ref 11) showed that the creep behavior of AZ91 alloy at 150 °C is greatly improved with the presence of Mg_2Si or Mg_3Sb_2 intermetallic phases because of their better thermal stability than $Mg_{17}Al_{12}$, and it was also found that these thermally stable intermetallics facilitates a greater number of continuous $Mg_{17}Al_{12}$ dynamic precipitates near the grain boundary during creep, which in turn restricts the creep deformation.

Mg alloys containing Mg_2Si precipitates with a high melting point of 1085 °C are receiving attention of design engineers as a promising light heat-resistant Mg alloy for automobile engine applications (Ref 12). However, increasing the amount of Si only increased the size and amount of the Mg_2Si precipitates, with no influence on the content or morphology of the $Mg_{17}Al_{12}$ phase, which is deleterious to the tensile properties of the matrix alloy, particularly its ductility (Ref 13, 14). With the development of nanotechnology, studies have reported that nano-sized SiC particles (n-SiCp) addition (Ref 15–21) could refine the grain size of the matrix and modify the morphology of the $Mg_{17}Al_{12}$ phase from coarse plates to lamellar precipitates, resulting in the simultaneous enhancement of ductility, strength and creep resistance. Among other things, the distribution and dispersion of the n-SiCp has a decisive effect on microstructure and mechanical properties of the nanocomposites. Nie et al. (Ref 22) demonstrated that semisolid stirring-assisted ultrasonic vibration is an inexpensive and effective

Ming Li, Southwest Technology and Engineering Research Institute, Chongqing 400039, People's Republic of China; and Shanxi Key Laboratory of Advanced Magnesium-Based Materials, School of Materials Science and Engineering, Taiyuan University of Technology, Taiyuan 030024, People's Republic of China; **Gaozhan Zhao, Zhiwei Huang, Jianquan Tao, Yuanyuan Wan, Zhihui Xing,** and **Qiang Chen**, Southwest Technology and Engineering Research Institute, Chongqing 400039, People's Republic of China; and **Hongxia Wang**, Shanxi Key Laboratory of Advanced Magnesium-Based Materials, School of Materials Science and Engineering, Taiyuan University of Technology, Taiyuan 030024, People's Republic of China. Contact e-mails: wanghxia1217@163.com and 2009chengqiang@163.com.

method to disperse the n-SiCp evenly within a matrix alloy. Therefore, preparing cost-effective n-SiCp-reinforced Mg matrix composites by semisolid stirring-assisted ultrasonic vibration appears to be a good alternative for improving the high-temperature applications of Mg-Al-based alloys.

In the light of the survey, most of the published works have concentrated on improving the tensile properties of n-SiCp-reinforced Mg matrix composites. In this work, it is endeavored to improve the creep resistance of Mg-9Al-1Si alloy by introducing the n-SiCp into the matrix. Semisolid stirring-assisted ultrasonic vibration is employed to fabricate the n-SiCp/Mg-9Al-1Si composites. The effect of SiC nanoparticles on the microstructure evolution and creep behavior of the n-SiCp/Mg-9Al-1Si composites was systematically investigated, and the strengthening effect of n-SiCp on the creep behavior of the nanocomposites was explained.

2. Experimental Procedures

In this paper, Mg-9Al-1Si alloy was selected as the matrix alloy, and SiC nanoparticles with an average size of 60 nm were chosen as the reinforcement. The volume content of n-SiCp in the n-SiCp/Mg-9Al-1Si composites was 0.5, 1, and 1.5%, respectively. The n-SiCp/Mg-9Al-1Si composites were fabricated by semisolid stirring-assisted ultrasonic vibration. The experimental setup for this study is given in Fig. 1. The detailed description of the fabrication process is described in Ref 23. Mg-9Al-1Si alloy was first melted in a crucible under a protective atmosphere of CO_2 and SF_6 and then cooled into a semisolid state. The n-SiCp were added into the semisolid slurry using a semisolid stirring technique. Then, the semisolid slurry was reheated into a liquid state and ultrasonically processed. Finally, the melt was cast into a preheated mold. For comparison, Mg-9Al-1Si alloy without n-SiCp was also fabricated under the same conditions.

Optical microscopy (OM), scanning electron microscopy (SEM) (MIRA 3XMU) equipped with energy dispersive spectroscopy (EDS) and transmission electron microscopy (TEM) (JEOL 2100F) were used to study the microstructure evolution of the matrix alloy and the distributions of SiC nanoparticles. The average grain size of the Mg-9Al-1Si alloy and its nanocomposites was analyzed from the microstructure images using the Image-Pro Plus software. The samples for OM and SEM observation were ground, polished and etched in acetic picral [10 mL glacial acetic acid + 5 g picric acid + 7 mL H_2O + 78 mL ethanol (95%)]. The specimens for TEM observation were ground until a foil of approximately 50 μm thickness was produced and then punched into 3-mm-diameter disks. Subsequently, the disks were thinned by ion beam.

Creep test samples were cut from the central part of the specimens by an electric discharge machine. Subsequently, the sample surfaces were polished mechanically with the 2000-grid emery paper before each creep test. The uniaxial tensile creep test was performed by a creep apparatus (RDL100, China) under an applied stress of 70 MPa at 200 °C. The temperature was constantly maintained within ± 2 °C of the target temperature throughout the tests.

3. Results and Discussion

3.1 Phase Composition Analysis

Figure 2 shows the x-ray diffraction patterns of the Mg-9Al-1Si alloy and its nanocomposites. Peak analysis shows that the

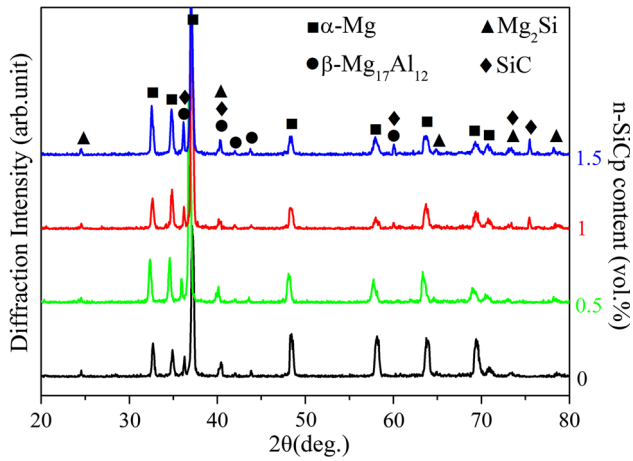

Fig. 2 XRD pattern of the Mg-9Al-1Si alloy and its nanocomposites

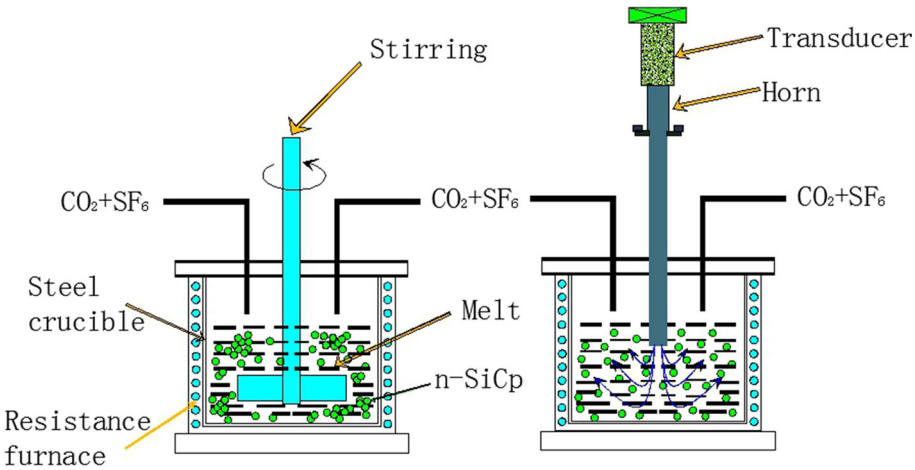

Fig. 1 Schematic diagram of the experimental setup for semisolid stirring-assisted ultrasonic vibration

Mg-9Al-1Si alloy consists of α-Mg, Mg_2Si, and $Mg_{17}Al_{12}$ phases, while α-Mg, Mg_2Si, $Mg_{17}Al_{12}$, and SiC phases are presented in all the nanocomposites. Note that the intensities of the SiC peak are very low, and only one or two peaks appear in the 0.5 and 1 vol.% n-SiCp/Mg-9Al-1Si composites due to their low contents within the matrix. According to the comparison of the XRD patterns to the ASTM cards, it is concluded that the SiC nanoparticle is in β-SiC phase with the face-centered cubic structure.

3.2 Microstructure Characterization

Figure 3 illustrates the OM micrographs of the Mg-9Al-1Si alloy and its nanocomposites fabricated by semisolid stirring-assisted ultrasonic vibration. The microstructure of the as-cast Mg-9Al-1Si alloy contains coarse primary α-Mg with an intermetallic-containing eutectic, as shown in Fig. 3(a). The intermetallics can be easily distinguished, with $Mg_{17}Al_{12}$ having a discontinuous netty shape and a blocky shape while Mg_2Si possesses a fishbone shape and a coarse Chinese script morphology. Compared with the Mg-9Al-1Si alloy, the phases of Mg_2Si and $Mg_{17}Al_{12}$ in the n-SiCp/Mg-9Al-1Si composites are obviously refined, as shown in Fig. 3(b)–(d). Moreover, all of the nanocomposites achieve significant grain refinement with the addition of the SiC nanoparticles. Figure 4 shows the average grain size of the Mg-9Al-1Si alloy and n-SiCp/Mg-9Al-1Si composites with different volume fractions. The average grain size of the Mg-9Al-1Si alloy is about 158 μm. With an increasing volume fraction of the n-SiCp, grain size of the matrix in the n-SiCp/Mg-9Al-1Si composite gradually decreased. A drastic reduction in the grain size of 59% is observed for the 1.5 vol.% n-SiCp/Mg-9Al-1Si composite. On the one hand, the number of active particles for effective heterogeneous nucleation increases with increasing the volume fraction of n-SiCp. On the other hand, the nanosized particles are pushed ahead of the solidification front by the liquid–solid interface, which in turn inhabits grain growth effectively during the solidification process (Ref 24).

Figure 5 shows the SEM microstructures of the Mg-9Al-1Si alloy and its nanocomposites. It is obviously seen that the morphology of $Mg_{17}Al_{12}$ and Mg_2Si is greatly dependent on the volume fraction of the n-SiCp. The size of the $Mg_{17}Al_{12}$ phase as well as the Mg_2Si phase is gradually decreased as the volume fraction of the n-SiCp increasing from 0 to 1%. Moreover, a change in morphology of the $Mg_{17}Al_{12}$ phase can be observed, where the massive $Mg_{17}Al_{12}$ shape was changed into a fine lamellar shape. The reason is that the n-SiCp can not

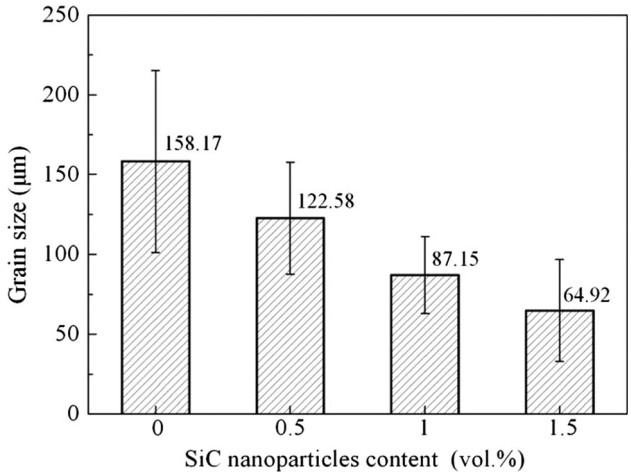

Fig. 4 Average grain size of Mg-9Al-1Si alloy and SiCp/Mg-9Al-1Si nanocomposite with different volume fractions

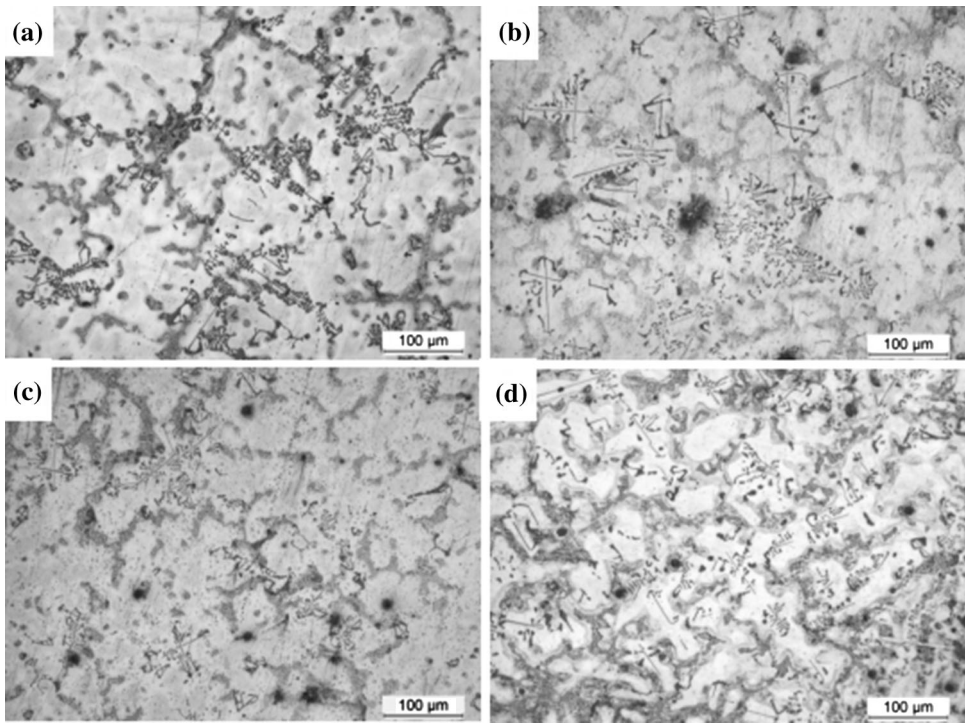

Fig. 3 Microstructure of (a) Mg-9Al-1Si alloy, (b) 0.5 vol.% SiCp/Mg-9Al-1Si nanocomposite, (c) 1 vol.% SiCp/Mg-9Al-1Si nanocomposite and (d) 1.5 vol.% SiCp/Mg-9Al-1Si nanocomposite

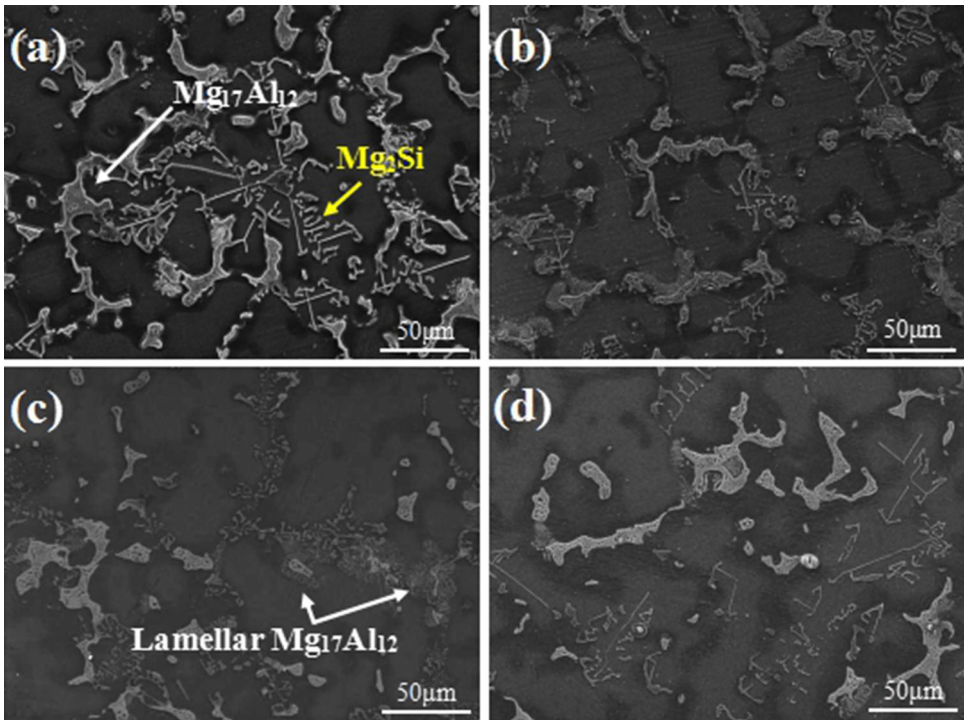

Fig. 5 Morphology and distribution of Mg_2Si and β-$Mg_{17}Al_{12}$ phase in (a) Mg-9Al-1Si alloy, (b) 0.5 vol.% SiCp/Mg-9Al-1Si nanocomposite, (c) 1 vol.% SiCp/Mg-9Al-1Si nanocomposite and (d) 1.5 vol.% SiCp/Mg-9Al-1Si nanocomposite

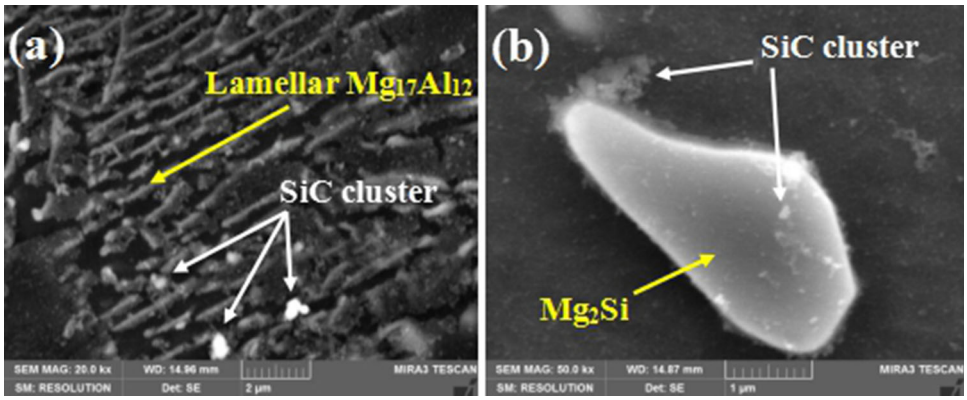

Fig. 6 SEM micrographs at higher magnification of (a) β-$Mg_{17}Al_{12}$ and (b) Mg_2Si phase in the 1 vol.% SiCp/Mg-9Al-1Si nanocomposite

only act as the nucleation sites for the heterogeneous nucleation of $Mg_{17}Al_{12}$ and Mg_2Si phases, but also hinder the growth of $Mg_{17}Al_{12}$ and Mg_2Si phases during the solidification process. As shown in Fig. 6, the refined $Mg_{17}Al_{12}$ and Mg_2Si phases contain a lot of n-SiCp inside, which act as nucleation sites for the $Mg_{17}Al_{12}$ and Mg_2Si phases. And the refined $Mg_{17}Al_{12}$ and Mg_2Si particles are surrounded by the SiC nanoparticles or clusters, which presumably act as a barrier restricting the growth of $Mg_{17}Al_{12}$ and Mg_2Si phases.

However, size coarsening of the $Mg_{17}Al_{12}$ and Mg_2Si phases is shown in Fig. 5(c) and (d) as the volume fraction of n-SiCp increases to 1.5%. The reason for this result is that the content of n-SiCp is high enough that it cannot be uniformly dispersed in the matrix by the semisolid stirring-assisted ultrasonic vibration, which in turn leads to the decreasing of nucleation sites for the $Mg_{17}Al_{12}$ and Mg_2Si phases. Figure 7 shows the distribution of n-SiCp in the n-SiCp/Mg-Al-Si composites. As shown in Fig. 7(a), most of n-SiCp exhibit a relatively uniform distribution in the 1 vol.% n-SiCp/Mg-9Al-1Si nanocomposite, and these nanoparticles bond well with the matrix. With the volume fraction of n-SiCp increasing to 1.5%, it is obvious that some of the SiC nanoparticles are evenly dispersed, while some are found to be severely agglomerated in the 1.5 vol.% SiCp/Mg-9Al-1Si nanocomposite, as shown in Fig. 7(b).

3.3 Creep Behavior

Figure 8 depicts representative creep curves of the Mg-9Al-1Si alloy and n-SiCp/Mg-9Al-1Si composites with different volume fractions obtained at 200 °C with an applied stress of 70 MPa. As can be seen, all the curves show typical three-stage creep characteristics, which consist of the primary, secondary and tertiary stages. Creep properties such as the steady-creep

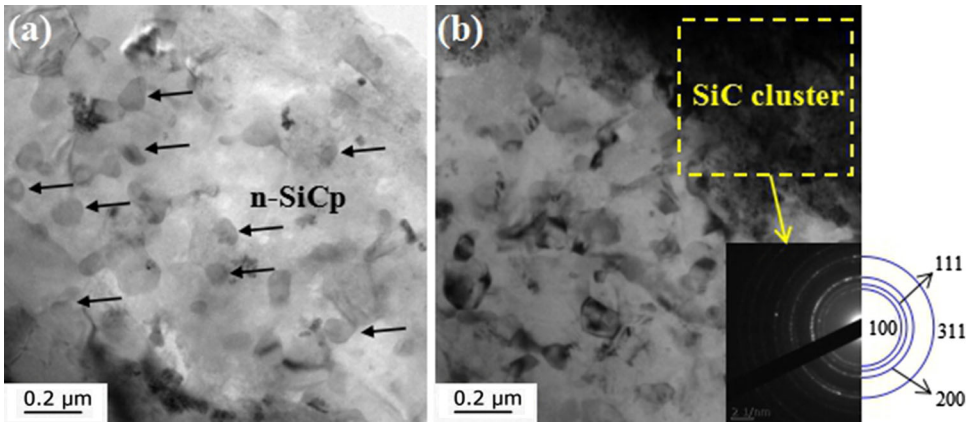

Fig. 7 TEM micrographs of (a) 1 vol.% SiCp/Mg-9Al-1Si nanocomposite and (b) 1.5 vol.% SiCp/Mg-9Al-1Si nanocomposite

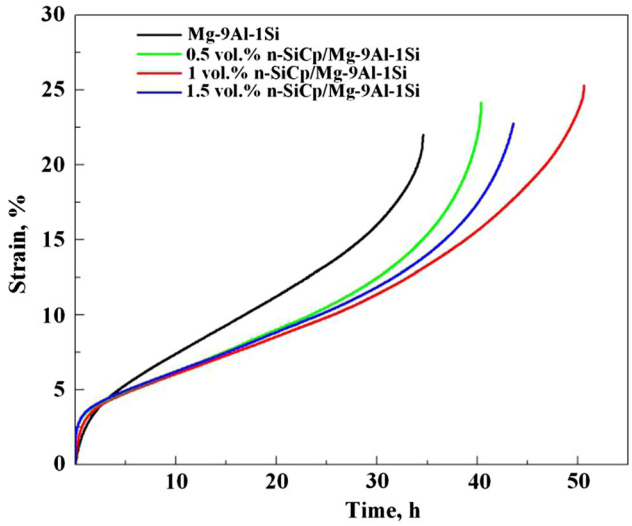

Fig. 8 Representative creep curves of Mg-9Al-1Si alloy and its nanocomposites at 200 °C and 70 MPa

Table 1 Creep properties of Mg-9Al-1Si alloy and its nanocomposites at 200 °C and 70 MPa

Materials	Steady-creep rate, s^{-1}	Creep strain, %	Creep life, h
Mg-9Al-1Si alloy	1.13×10^{-6}	21.97	34.61
0.5 vol.% n-SiCp/Mg-9Al-1Si	8.67×10^{-7}	24.16	40.38
1 vol.% n-SiCp/Mg-9Al-1Si	6.94×10^{-7}	25.30	50.59
1.5 vol.% n-SiCp/Mg-9Al-1Si	7.92×10^{-7}	22.75	43.57

rate, creep strain and creep life obtained from the creep results are given in Table 1. It is clear that the creep strain as well as the creep life of the n-SiCp/Mg-9Al-1Si composites is gradually increased as the volume fraction of n-SiCp increasing from 0 to 1%. Moreover, compared to the Mg-9Al-1Si alloy, the steady-creep rate of all of the nanocomposites is significantly decreased with the addition of the SiC nanoparticles. A drastic reduction in the steady-creep rate of 38.6% is observed for the 1 vol.% n-SiCp/Mg-9Al-1Si composite. That is, the reinforced SiC nanoparticles exhibit a great strengthening effect on the creep behavior of the Mg-9Al-1Si matrix alloy. The reason for the improved creep properties is mainly attributed to basic strengthening mechanisms, such as (i) the Hall–Petch effect due to the grain refinement as shown in Fig. 4; (ii) the Orowan strengthening mechanism due to the uniform distribution of n-SiCp in the matrix alloy as shown in Fig. 7(a); and (iii) the load transfer effect due to the good interfacial bonding between the matrix and n-SiCp as shown in Fig. 7(a). Moreover, the presence of hard and thermally stable n-SiCp distributed inside the grains as well as along the grain boundaries acts as strong obstacles to impeding the movement of dislocations and thus inhibits the slip insider the grains during dislocation creep regimes, and also restricts the grain boundary migration or grain boundary sliding during creep deformation (Ref 25). However, as the volume fraction of n-SiCp increased to 1.5%, the creep strain as well as the creep life had a evident decline, and the steady-creep rate increased obviously. This could be attributed to a decrease in the amount of refined $Mg_{17}Al_{12}$ and Mg_2Si phases and an increase in the agglomeration of n-SiCp, as shown in Fig. 5 and 7(b).

Figure 9 illustrates the creep fractured microstructures (parallel to the tensile direction) of the Mg-9Al-1Si alloy and n-SiCp/Mg-9Al-1Si composites with different volume fractions at 200 °C and 70 MPa. It is observed that micro-cracks propagate along the blocky $Mg_{17}Al_{12}$ phase. This is due to the uncoordinated deformation between the blocky $Mg_{17}Al_{12}$ phase and the matrix alloy during creep deformation. The temperature stability of these blocky $Mg_{17}Al_{12}$ phases is poor and their low melting point results in the coarsening and dissolution of the thermally unstable $Mg_{17}Al_{12}$ intermetallic phase at elevated temperatures. In addition, the size and number of holes in the matrix decrease significantly as the volume fractions of the n-SiCp increase, as indicated in Fig. 9. It can be explained that the thermally stable n-SiCp and the refined $Mg_{17}Al_{12}$ and Mg_2Si phases strengthen the grain boundary against sliding and hence reduce the creep damage and the possibility of hole propagation sites during the creep process.

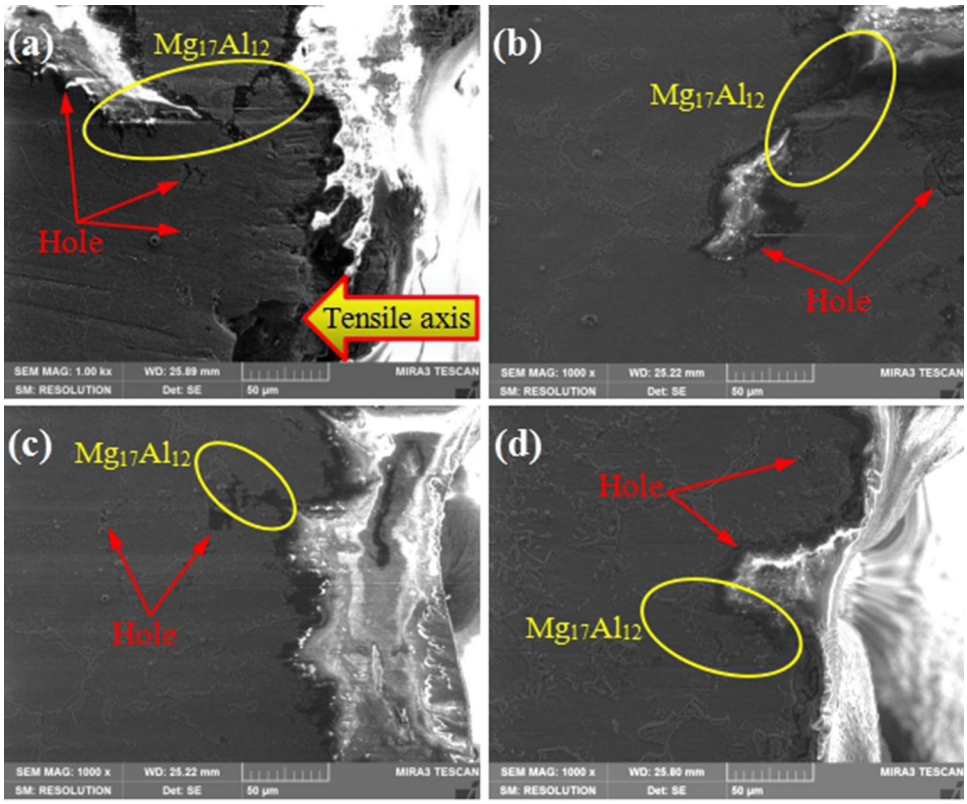

Fig. 9 SEM micrographs of (a) Mg-9Al-1Si alloy, (b) 0.5 vol.% SiCp/Mg-9Al-1Si nanocomposite, (c) 1 vol.% SiCp/Mg-9Al-1Si nanocomposite and (d) 1.5 vol.% SiCp/Mg-9Al-1Si nanocomposite after creep testing at 200 °C and 70 MPa

4. Conclusion

The effects of reinforcing nano-sized SiCp on the microstructure characterization and creep behavior of the n-SiCp/Mg-9Al-1Si composites were systematically investigated. The conclusions from this work can be summarized by the following:

(1) With the addition of SiC nanoparticles, the n-SiCp/Mg-9Al-1Si composites exhibit a uniform microstructure, in which the grains and most of the $Mg_{17}Al_{12}$ and Mg_2Si phases in the nanocomposite are gradually refined compared with the Mg-9Al-1Si alloy. Most of n-SiCp exhibit a relatively uniform distribution in the 1 vol.% n-SiCp/Mg-9Al-1Si composite, and the nanoparticles bond well with the matrix. When the volume fraction of the n-SiCp increases to 1.5%, the sizes of the $Mg_{17}Al_{12}$ and Mg_2Si phases increase significantly and some of the n-SiCp are found to be severely agglomerated in the 1.5 vol.% n-SiCp/Mg-9Al-1Si composite.

(2) The creep rupture life of the 1 vol.% n-SiCp/Mg-9Al-1Si composite crept at 200 °C and 70 MPa is approximately 1.5 times longer than that of the Mg-9Al-1Si alloy. The steady-creep rate of the n-SiCp/Mg-9Al-1Si composite is reduced by 38.6% compared to that of the Mg-9Al-1Si alloy.

Acknowledgments

This work was supported by the National Natural Science Foundation of China (Nos. 51301118, 51375464 and 51404166), the National Natural Science Foundation of Shanxi Province (No. 201701D121045), Shanxi Province Scientific Facilities and Instruments Shared Service Platform (No. 201805D141005) and the Shanxi Key Laboratory of Advanced Magnesium-Based Material, Taiyuan University of Technology (AMM-2017-12).

References

1. K.B. Nie, X.J. Wang, K. Wu, X.S. Hu, and M.Y. Zheng, Development of SiCp/AZ91 Magnesium Matrix Nanocomposites Using Ultrasonic Vibration, *Mater. Sci. Eng., A*, 2012, **540**, p 123–129
2. Q. Chen, Z.D. Zhao, G. Chen, and B. Wang, Effect of Accumulative Plastic Deformation on Generation of Spheroidal Structure, Thixoformability and Mechanical Properties of Large-Size AM60 Magnesium Alloy, *J. Alloys Compd.*, 2015, **632**, p 190–200
3. X.G. Qiao, T. Ying, M.Y. Zheng, E.D. Wei, K. Wu, X.S. Hu, W.M. Gan, H.G. Brokmeier, and I.S. Golovin, Microstructure Evolution and Mechanical Properties of Nano-SiCp/AZ91 Composite Processed by Extrusion and Equal Channel Angular Pressing (ECAP), *Mater. Charact.*, 2016, **121**, p 222–230
4. L. Zhang, Q.D. Wang, W.J. Liao, W. Guo, B. Ye, H.Y. Jiang, and W.J. Ding, Effect of Homogenization on the Microstructure and Mechanical Properties of the Repetitive-Upsetting Processed AZ91D Alloy, *J. Mater. Sci. Technol.*, 2017, **33**, p 935–940
5. L.W. Zheng, H.H. Nie, W.G. Zhang, W. Liang, and Y.D. Wang, Microstructural Refinement and Improvement of Mechanical Properties of Hot-Rolled Mg-3Al-Zn Alloy Sheets Subjected to Pre-extrusion and Al-Si Alloying, *Mater. Sci. Eng., A*, 2018, **722**, p 58–68
6. K.B. Nie, K.K. Deng, X.J. Wang, F.J. Xu, K. Wu, and M.Y. Zheng, Multidirectional Forging of AZ91 Magnesium Alloy and its Effects on Microstructures and Mechanical Properties, *Mater. Sci. Eng., A*, 2015, **624**, p 157–168
7. Z.Y. Zhang, H.S. Yu, G. Chen, H. Yu, and C.Z. Xu, Correlation Between Microstructure and Tensile Properties in Powder Metallurgy AZ91 Alloy, *Mater. Lett.*, 2011, **65**, p 2686–2689

8. S.M. Zhu, M.A. Gibson, M.A. Easton, and J.F. Nie, The Relationship Between Microstructure and Creep Resistance in Die-cast Magnesium-Rare Earth Alloys, *Scripta Mater.*, 2010, **63**, p 698–703
9. B.L. Mordike, Creep-Resistant Magnesium Alloys, *Mater. Sic. Eng. A*, 2002, **324**, p 103–112
10. K.M. Asl, A. Tari, and F. Khomamizadeh, The Effect of Different Content of Al, RE, and Si Element on the Microstructure, Mechanical and Creep Properties of Mg-Al Alloys, *Mater. Sic. Eng. A*, 2009, **523**, p 1–6
11. A. Srinivasana, J. Swaminathanb, M.K. Gunjanb, U.T.S. Pillai, and B.C. Paia, Effect of Intermetallic Phases on the Creep Behavior of AZ91 Magnesium Alloy, *Mater. Sic. Eng. A*, 2010, **527**, p 1395–1403
12. P.S. Roodposhti, A. Sarkar, K.L. Murty, and R.O. Scattergood, Effects of Microstructure and Processing Methods on Creep Behavior of AZ91 Magnesium Alloy, *J. Mater. Eng. Perform.*, 2016, **25**, p 3697–3709
13. A. Srinivasana, U.T.S. Pillai, and B.C. Paia, Effect of Elemental Additions (Si and Sb) on the Ageing Behavior of AZ91 Magnesium Alloy, *Mater. Sic. Eng. A*, 2010, **527**, p 6543–6550
14. Z. Trojanová, V. Gärtnerová, A. Jäger, A. Námešný, M. Chalupová, P. Palček, and P. Lukáč, Mechanical and Fracture Properties of an AZ91 Magnesium Alloy Reinforced by Si and SiC Particles, *Compos. Sci. Technol.*, 2009, **69**, p 2256–2264
15. G. Cao, H. Konishi, and X. Li, Mechanical Properties and Microstructure of SiC-Reinforced Mg-(2,4)Al-1Si Nanocomposites Fabricated by Ultrasonic Cavitation Based Solidification Processing, *Mater. Sci. Eng., A*, 2008, **486**, p 357–362
16. K.B. Nie, X.J. Wang, X.S. Hu, L. Xu, K. Wu, and M.Y. Zheng, Microstructure and Mechanical Properties of SiC Nanoparticles Reinforced Magnesium Matrix Composites Fabricated by Ultrasonic Vibration, *Mater. Sci. Eng., A*, 2011, **528**, p 5278–5282
17. L.Y. Chen, J.Q. Xu, H. Choi, M. Pozuelo, X.L. Ma, S. Bhowmick, J.M. Yang, S. Mathaudhu, and X.C. Li, Processing and Properties of Magnesium Containing a Dense Uniform Dispersion of Nanoparticles, *Nature*, 2015, **528**, p 539–543
18. Q. Chen, G. Chen, L.N. Han, N. Hu, F. Han, Z.D. Zhao, X.S. Xia, and Y.Y. Wan, Microstructure Evolution of SiCp/ZM6 (Mg-Nd-Zn) Magnesium Matrix Composite in the Semi-solid State, *J. Alloys Compd.*, 2016, **656**, p 67–76
19. H. Zhang, Y.C. Zhao, Y. Yan, J.F. Fan, L.F. Wang, H.B. Dong, and B.S. Xu, Microstructure Evolution and Mechanical Properties of Mg Matrix Composites Reinforced with Al and Nano SiC Particles Using Spark Plasma Sintering Followed by Hot Extrusion, *J. Alloys Compd.*, 2017, **725**, p 652–664
20. S. Kamrani, D. Penther, A. Ghasemi, R. Riedel, and C. Fleck, Microstructural Characterization of Mg-SiC Nanocomposite Synthesized by High Energy Ball Milling, *Adv. Powder Technol.*, 2018, **29**, p 1742–1748
21. G. Li, M. Li, H.X. Wang, Z.Y. Zhang, W.L. Cheng, W. Liang, and C.J. Zhang, Dependence of Microstructure Characteristics and Mechanical Properties on Nanosize SiCp Contents in Mg-9Al Matrix Composites Fabricated by Ultrasonic-Assisted Semisolid Powder Hot Pressing, *J. Mater. Res.*, 2018, **33**, p 2689–2699
22. K.B. Nie, X.J. Wang, K. Wu, L. Xu, M.Y. Zheng, and X.S. Hu, Processing, Microstructure and Mechanical Properties of Magnesium matrIx Nanocomposites Fabricated by Semisolid Stirring Assisted Ultrasonic Vibration, *J. Alloys Compd.*, 2011, **509**, p 8664–8669
23. S.X. Zhang, M. Li, H.X. Wang, W.L. Cheng, W.W. Lei, Y.M. Liu, and W. Liang, Microstructure and Tensile Properties of ECAPed Mg-9Al-1Si-1SiC Composites: The Influence of Initial Microstructures, *Materials*, 2018, **11**, p 136. https://doi.org/10.3390/ma11010136
24. B.F.S. Chultz, J.B. Ferguson, and P.K. Rohatgi, Microstructure and Hardness of Al_2O_3 Nanoparticle Reinforced Al-Mg Composites Fabricated by Reactive Wetting and String Mixing, *Mater. Sci. Eng., A*, 2011, **530**, p 87–97
25. W.S. Tian, Q.L. Zhao, Q.Q. Zhang, F. Qiu, and Q.C. Jiang, Superior creep resistance of 0.3 wt.% nano-sized TiCp/Al-Cu composite, *Mater. Sic. Eng. A*, 2017, **700**, p 42–48